

# Reappraisal of trifluoperidol against Nsp3 as a potential therapeutic for novel COVID-19: a molecular docking and dynamics study

Ajita Pandey\*<sup>1</sup> & Mohit Sharma<sup>2</sup><sup>1</sup>School of Biotechnology, Gautam Buddha University, Greater Noida, Uttar Pradesh, India<sup>2</sup>School for Molecular Medicine, Warszawskiego Uniwersytetu Medycznego, Warsaw, Poland\*Author for correspondence: +91 958 204 1608; [ajitanu5@gmail.com](mailto:ajitanu5@gmail.com)

Novel COVID-19 is a highly infectious disease that is caused by the recently discovered SARS-CoV-2. It is a fast-spreading disease that urgently requires therapeutics. The current study employed computational regression methods to target the ADP-ribose phosphatase (ADRP) domain of Nsp3 using FDA-approved drugs. Identified leads were further investigated using molecular dynamics simulation (MDS). The screening and MDS results suggest that trifluoperidol could be a novel inhibitor of the ADRP domain of Nsp3. Trifluoperidol could, therefore, be used to help control the spread of COVID-19, either alone or in combination with antiviral agents.

First draft submitted: 27 October 2020; Accepted for publication: 14 June 2021; Published online: 13 July 2021

**Keywords:** ADRP • FDA drugs • molecular docking • molecular dynamic simulation • Nsp3 • PCA • SARS-CoV-2

In December 2019, a number of cases of pneumonia occurred in Wuhan (Hubei Province, China), with the first patient being hospitalized on 12 December 2019 [1]. Physician Li Wenliang was the first to suspect that these cases of pneumonia were caused by a coronavirus and, on 31 December 2019, the Chinese Center for Disease Control and Prevention and the Chinese office of the WHO officially confirmed the existence of a new coronavirus. The new virus, which was named 'severe acute respiratory syndrome coronavirus-2' (SARS-CoV-2), causes a highly infectious disease, termed 'novel coronavirus disease 2019' (COVID-19), which often presents with pneumonia-like symptoms. SARS-CoV-2 is closely related to other coronaviruses, such as SARS-CoV and pangolin coronaviruses [2]. SARS-CoV-2 spread very rapidly and COVID-19 quickly became a global pandemic. As of 5 June 2021, the WHO has confirmed 173,483,489 cases of COVID-19 worldwide, with 3,731,545 deaths (<https://www.worldometers.info/coronavirus/>). COVID-19 is now spreading rapidly in India, with thousands of new cases reported daily. As of 5 June 2021, more than 28,775,440 confirmed cases and 3,45,055 deaths (<https://www.covid19india.org/>) have been reported.

Like other coronaviruses, SARS-CoV-2 has a positive-sense RNA genome and encodes several structural and non-structural proteins (Nsp3). The structural proteins include the envelope, glycoprotein, nucleocapsid and membrane proteins, together with other accessory proteins [3]. The ORF1a and ORF1ab open reading frames are translated to produce two polyproteins, pp1a and pp1ab, which are cleaved by proteases encoded by ORF1a to yield the Nsps [4]. The latter polyprotein results from a ribosomal frameshift that enables continuous translation of ORF1a along with ORF1b. The polyprotein pp1a contains two viral proteases, a papain-like protease (PLpro, encoded within Nsp3) and a 3C-like main protease (Mpro, encoded by Nsp5). These two viral proteases play key roles in the post-translation processing of the two polyproteins. The 16 Nsps that are formed by cleavage form a large membrane-bound replicase complex [5]. The multidomain protein Nsp3, which is the largest component in the replicase assembly, consists of an ADP-ribose phosphatase (ADRP) domain, also known as the macrodomain, an N-terminal Nsp3a domain, a PLpro domain, a marker domain, a SARS-unique domain, an RNA binding domain, a Y-domain and a transmembrane domain (<https://coronavirus3d.org>). Thirty years ago, the ADRP domain (initially known as the X domain) was shown, using bioinformatics techniques, to be a conserved and unique domain in the genomes of the Coronaviridae, Togaviridae and Hepeviridae families [6]. The ADRP domain is involved in

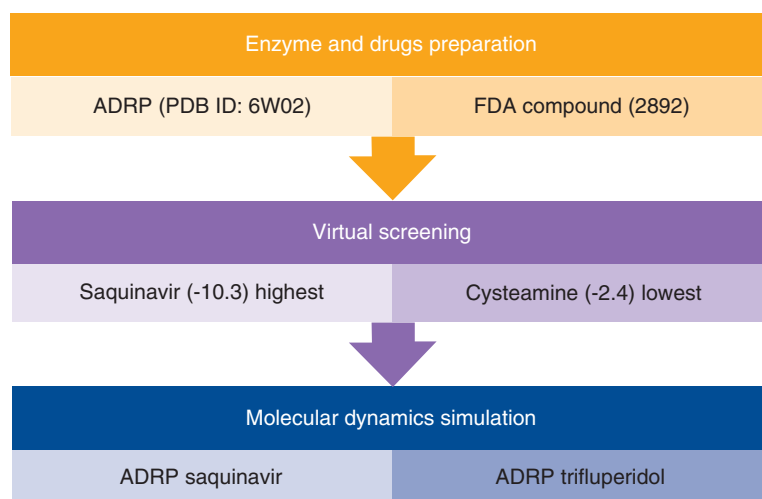


**Figure 1. Complete workflow of screening methodology.** ADRP: ADP-ribose phosphatase; PDB: Protein Data Bank.

various pathways, including post-translational modification of proteins and ADP-ribose metabolism. The Nsp3 protein removes the 1'' phosphate group from Appr-1''-p in *in vitro* assays, confirming its phosphatase activity [7]. It is believed that the ADRP domain plays a key role in altering innate immunity. Studies to investigate the role of this domain in compromising the immune response have shown that virus with a mutated macrodomain replicated poorly in bone marrow-derived macrophages, which are the primary cells involved in mounting an innate immune response [8]. Virus containing an inactivated macrodomain was also shown to be sensitive to pretreatment with interferon [9]. These studies confirm that the ADRP domain plays a crucial role in disease pathogenesis and suggest that inhibition of this domain should reduce viral burden and facilitate recovery [10].

Numerous studies have been conducted using different coronavirus proteins as drug targets [11–13]. But, to the best of our knowledge, no studies have examined the proteins involved in modifying host innate immunity. In the current study the authors choose to identify compounds that interact with the ADRP domain as potential antiviral agents. Virtual screening of 2892 FDA-approved drugs was conducted, using the ADRP domain in the adenosine-5-diphosphoribose (ADPr) centric grid. Using a variety of computational methods, trifluoperidol was found to be a potential hit, and could be repurposed to treat COVID-19. The comprehensive methodology is shown in Figure 1.

## Experimental procedures

### Protein preparation

The ADRP domain (PDB ID: 6W02, x-ray, 1.5 Å), which is a subunit of Nsp3, was retrieved from the Protein Data Bank (PDB) and used for protein preparation [10]. Cococrystallization of the ADRP domain with ADPr revealed interactions with the key catalytic residues. We removed all heteroatoms, water molecules and other unnecessary crystal stabilizers, then prepared the protein using Chimera 1.13.2 [14]. The protein was imported into Chimera and minimized with the Amber ff99SB force field, using the 100 steepest descent steps with 10 conjugant gradient steps to obtain the lowest and most stable conformation of the protein. The step size for both methods was set at 0.02 Å. The minimized lowest-energy conformation and prepared structure were used for virtual screening.

### Ligand preparation

All 2892 FDA-approved drugs were retrieved from the Drug Bank database (<https://www.drugbank.ca/>), which contains all FDA-approved drugs, as well as experimental and withdrawn compounds [15]. The same compounds are also available in the ZINC database [16] in mol2 file format, and are ready to use without preparation. The FDA-approved compounds were retrieved in 3D SDF format and then converted to .mol2 file format using Open Bable software [17]. The .mol2 files were then converted into .pdbqt file format using a Python script. During assignment of Gastieger charges, all hydrogen atoms and atomic radii were added in the course of ligand preparation. The converted and prepared ligands were then used for virtual screening.

### Structure-based virtual screening

Structure-based virtual screening (SBVS) is a powerful computational technique for identifying compounds on the basis of binding affinity [18,19]. SBVS was used to predict which compounds might bind to the ADRP domain of Nsp3. The crystal structure of ADPr bound to the ADRP domain showed that the binding site comprised residues Ala21, Asp22, Ile23, Ala38, Asn40, Lys44, His45, Gly46, Gly47, Gly48, Val49, Leu126, Ser128, Ala129, Gly130, Ile131, Phe132, Ala154, Phe156 and Leu160. A centric grid box toward ADPr was then prepared on the basis of these catalytic residues. The protein structure of the ADRP domain was prepared using MGL Tools [20]. Hydrogen atoms and Kollman charges were added during protein preparation. The prepared structure of the ADRP domain was then converted into .pdbqt file format and used for virtual screening. Autodock Vina (Scripps Research, CA, USA) [21], which is widely used for virtual screening, was used in this study. The centric grid size in the ADPr-binding cavity was 28, 26, and 52 Å, centralized at 3.941, 5.589 and 22.719 for x, y and z coordinates, respectively. The exhaustiveness and grid spacing were set to 8 and 1.00 Å, respectively, for screening. Compounds with the best binding were short listed on the basis of binding affinity and binding pose. The top few compounds were manually analyzed and only those compounds that bound to the catalytic residues and had greater binding affinity than the substrate were selected for further analysis.

### Analysis of docking complex

The docking complex was analyzed using Chimera 1.13.2 and Discovery Studio Visualizer (Dassault Systèmes, Vélizy-Villacoublay, France) and the 5 Å residues were selected to illustrate ADRP-drug interactions. Chimera was also used to generate the charged potential surface of the protein to show how the ligands bind in the deep cavity of the ADRP domain. A detailed 2D-interaction diagram was generated using Discovery Studio Visualizer, which displays various interactions, such as hydrogen bonds, interactions with halogen and alkyl groups and van der Waals interactions. This interaction analysis was carried out to determine whether or not the predicted drugs bind to the catalytic residues.

### Conformational analysis

Molecular dynamics simulation (MDS) is widely used to investigate the conformational dynamics and stability of protein–ligand complexes [22,23] and can describe atomic-level changes over time following ligand binding [24,25]. MDS was used to track atomic changes and to predict the stability of the protein–ligand complexes. The two drug complexes (ADRP–saquinavir and ADRP–trifluoperidol) and the substrate complex ADRP–ADPr were used for 100 ns MDS analysis using Gromacs [26]. The topology of the ligands was generated using the ProDRG server [27] and protein topology was generated with the GROMOS 9653a6 force field [28], using Gromacs. All the systems were placed in a dodecahedron box and solvated using the SPC water model. The systems were then neutralized by addition of 0.15 nM Na<sup>+</sup> and Cl<sup>-</sup> ions and used for energy minimization. The energy minimization removed all steric hindrances and clashes of systems that appeared after addition of solvent and ions. Number of particles, volume and temperature (NVT); and number of particles, pressure and temperature (NPT) simulations of 100 ps were then carried out to fix the volume, temperature and pressure of all the systems. These equilibrated systems were then used for the final production run of 100 ns, and the trajectories were recorded in 2 fs intervals.

### Analysis of MDS

The trajectories were preprocessed using the gmxtrjconv tool before analysis, as described earlier [29,30]. The artifacts and periodic boundary condition errors were removed from the trajectory and the processed trajectories were used for further analysis. Various types of analysis were carried out to predict the dynamics of the systems. The gmxrms, gmxrmsf, gmx gyration, gmxsasa and gmxhbond functions were used to analyze root mean square deviation, root mean square fluctuation, solvent-accessible surface area and hydrogen bonds, respectively. Principal component analysis (PCA) was carried out using the gmxcovar and gmxanaeig tools of Gromacs to understand the correlated motions that are induced after ligand binding. The trajectories were visualized using Chimera [31] and Visual Molecular Dynamics software [32].

### Analysis of binding free energy

The molecular mechanics–Poisson–Boltzmann surface area (MM-PBSA) was calculated using the g\_mmpbsa tool developed by Kumari *et al.* [33], which predicts different energy components, such as hydrophobic and electrostatic interactions, and solvent-accessible surface area (SASA). We used the last 5 ns stable trajectory snapshots to calculate

**Table 1. FDA-approved drugs showing remarkable binding affinity to the ADRP macrodomain of Nsp3.**

	ZINC ID	Drug Bank ID	Drug name	Binding affinity (kcal/mol)	Therapeutics
1.	ZINC03914596	DB01232	Squanavir	-10.3	HIV-1 protease inhibitor.
2.	ZINC00538505	DB13552	Trifluoperidol	-10.2	Used in the treatment of psychoses including mania and schizophrenia.
3.	ZINC01481815	DB01609	Deferasirox	-10	Used as an iron chelator.
4.	ZINC19796080	DB00450	Droperidol	-10	Used to maintain patient in a calm state of neuroleptanalgesia with indifference to surroundings.
5.	ZINC00968279	DB00197	Troglitazone	-9.9	Used for Type II diabetes mellitus (now withdrawn).
6.	ZINC11616581	DB01252	Mitiglinide	-9.8	Used for Type II diabetes mellitus.
7.	ZINC01481956	DB01267	Paliperidone	-9.7	Used for neurological disorders.
8.	ZINC01489478	DB01261	Sitagliptin	-9.7	Used for Type II diabetes mellitus.
9.	ZINC05844792	DB04861	Nebivolol	-9.6	Used for kidney disorder
10.	ZINC01996117	DB00496	Darifenacin	-9.5	Used for the treatment of urinary incontinence.
11.	ZINC03817234	DB04835	Celsentri	-9.5	Used in the treatment of HIV.
12.	ZINC03830974	DB01167	Itraconazole	-9.5	Used for fungal infection.
13.	ZINC03869855	DB00266	Dicumarol	-9.5	Used as an oral anticoagulant agent.
14.	ZINC06716957	DB04868	Nilotinib	-9.5	Acts as a tyrosine kinase inhibitor; possible medication for chronic myelogenous leukemia.
15.	ZINC00523926	DB01120	Gliclazide	-9.4	Used for the treatment of non-insulin-dependent diabetes mellitus.
16.	ZINC00601317	DB01501	Difenoxin	-9.4	Used as an antidiarrheal drug.
17.	ZINC03831258	DB04823	Oxyphenisatine	-9.4	A laxative that undergoes enterohepatic circulation.
18.	ZINC18098320	DB00878	Chlorhexidine	-9.4	Acts as an antimicrobial agent (generally used by dentists).
19.	ZINC01550477	DB01259	Lapatinib	-9.4	An anticancer drug.
20.	ZINC03871723	DB04794	Bifonazole	-9.3	An azole antifungal drug.

the binding free energy. The binding energy of the complex was calculated using the following equation:

$$\Delta G_{\text{Binding}} = G_{\text{Complex}} - (G_{\text{Protein}} + G_{\text{Ligand}})$$

where  $G_{\text{Complex}}$  is the total free energy of the binding complex,  $G_{\text{Protein}}$  and  $G_{\text{Ligand}}$  are the total free energies of the protein and ligand, respectively, and  $\Delta G_{\text{Binding}}$  is the total binding energy.

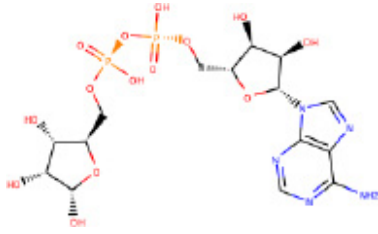
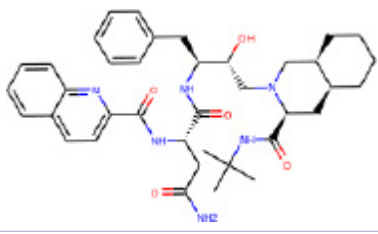
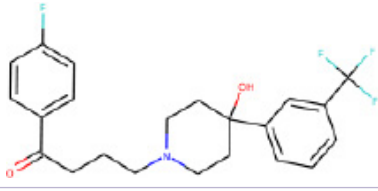
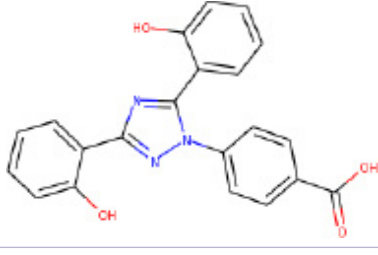
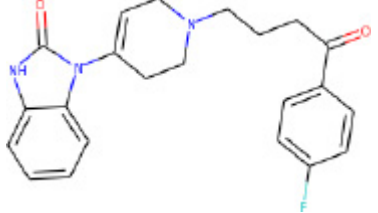
## Results

### Virtual screening

Virtual screening was carried out to identify compounds that bind to the ADRP macrodomain subunit of the SARS-CoV-2 Nsp3 enzyme. The binding energies of the 2892 FDA-approved drugs were between -10.3 and -2.5 kcal/mol. In the virtual screening, saquinavir had the highest binding energy (-10.3 kcal/mol) and cysteamine had the lowest binding energy (-2.5 kcal/mol). The top 20 compounds that showed higher binding affinity than the substrate were selected (Table 1). These top 20 compounds showed binding affinities in the range of -10.3 to -9.5 kcal/mol, which is higher than that of the control compound ADPr (-9.1 kcal/mol). The top 20 compounds are all FDA-approved drugs and are used in a wide range of therapeutic settings (Table 1). The top four were selected on the basis of binding affinity and analyzed in more detail. The detailed interaction analysis showed that all these compounds bind to the key catalytic residues located within the deep binding groove of the protein. Drug names, detailed interactions and binding affinities are provided in Table 2.

### Analysis of interactions

The top four compounds were selected and their interactions with ADPr were compared. The results are described next.

Table 2. Common name of drug, structure and binding affinity from Autodock Vina and interacting residues.			
Drug Name	Structure	Binding energy	Residues
Aenosine-5-diphosphoribose		-9.1	Ala21, Asp22, Ile23, Ala38, Asn40, Lys44, His45, Gly46, Gly47, Gly48, Val49, Leu126, Ser128, Ala129, Gly130, Ile131, Phe132, Ala154, Phe156, Leu160
Saquinavir		-10.3	Asp22, Ile23, Ala38, Asn40, Gly46, Gly48, Gly47, Val49, Ala52, Pro125, Leu126, Ser128, Ala129, Gly130, Ile131, Phe132, Ala154, Asp157, Phe156
Trifluoperidol		-10.2	Asp22, Ile23, Ala38, Asn40, Gly46, Gly47, Gly48, Val49, Gly51, Ala52, Pro125, Leu126, Ser128, Ala129, Gly130, Ile131, Phe132, Ala154, Val155, Phe156, Asp157
Deferasirox		-10.0	Ala38, Gly48, Val49, Pro125, Leu126, Ser128, Ala129, Gly130, Ile131, Phe132, Gly133, Val155, Phe156, Asp157, Leu160
Droperidol		-10.0	Ile23, Ala38, Gly48, Val49, Pro125, Leu126, Ser128, Ala129, Gly130, Ile131, Phe132, Ala154, Val155, Phe156, Asp157, Leu160

### ADRP–ADPr

The crystal structure of the ADRP–ADPr complex was analyzed and compared with the binding of the docked ligands. The ADRP–ADPr complex showed 12 hydrogen bonds between ADPr and various residues in the ADRP domain and was also stabilized by other interactions between the ligand and ADRP domain. The residues involved in binding of ADPr to ADRP were Ala21, Asp22, Ile23, Ala38, Asn40, Lys44, His45, Gly46, Gly47, Gly48, Val49, Leu126, Ser128, Ala129, Gly130, Ile131, Phe132, Ala154, Phe156 and Leu160.

### ADRP–saquinavir

Saquinavir, an antiviral drug that is used to control HIV, was the top compound in the virtual screen. Saquinavir showed higher binding affinity than the control compound ADPr, indicating that it can bind competitively in the active site and inhibit the function of the ADRP macrodomain of Nsp3. The complex, which has a binding affinity

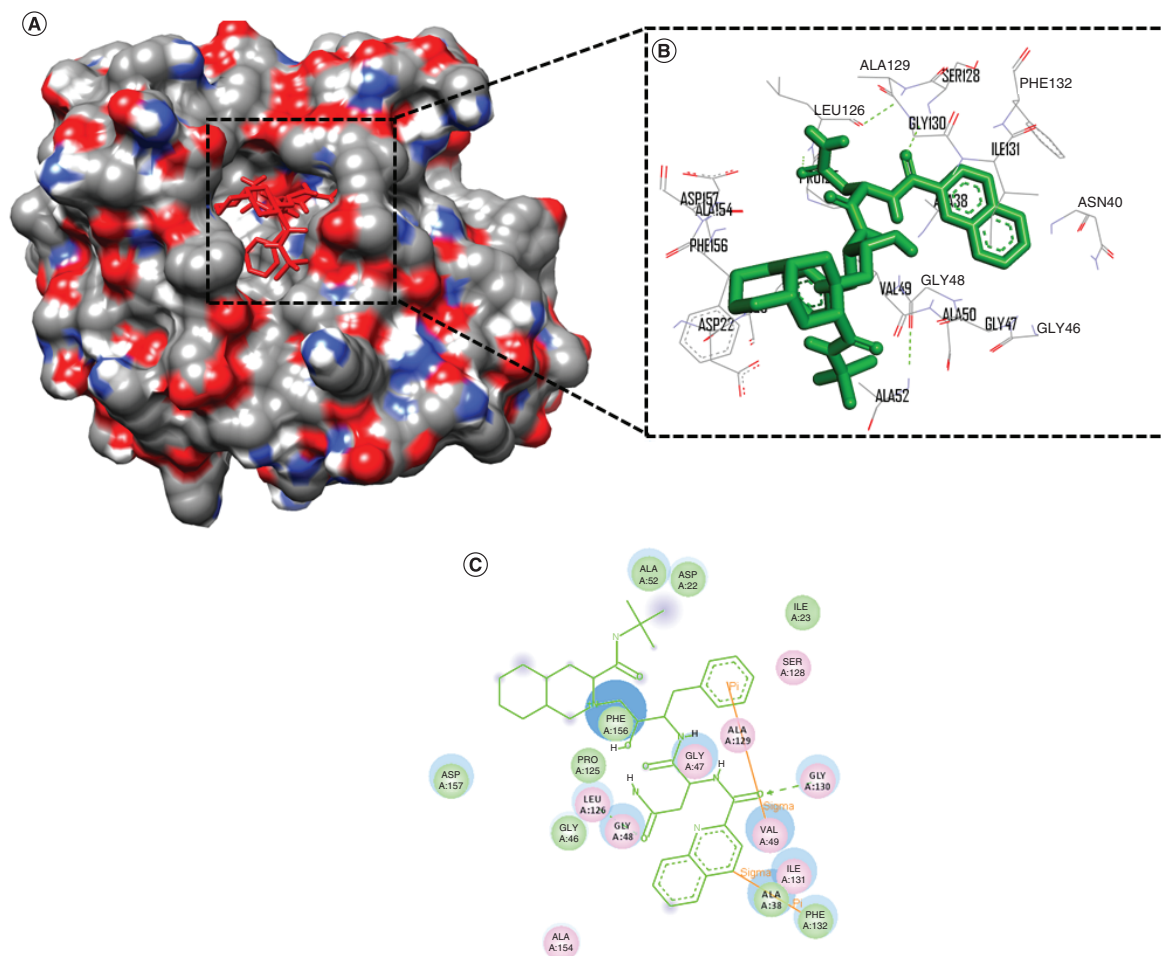


**Figure 2.** Binding pattern of saquinavir with ADP-ribose phosphatase. (A) Surface view of ADP-ribose phosphatase (ADRP)-saquinavir complex. (B) Residue interaction diagram of saquinavir with ADRP. (C) 2D-interaction diagram of ADRP-saquinavir interaction.

of  $-10.3$  kcal/mol, shows interactions between saquinavir and various key catalytic residues and is also stabilized by several other interactions. Gly130 and Leu126 form hydrogen bonds with saquinavir, and Val49 and Phe132 form  $\pi$  and  $\sigma$  interactions with saquinavir. Other residues, including Asp22, Ile23, Ala38, Asn40, Gly46, Gly48, Gly47, Ala52, Pro125, Ser128, Ala129, Ile131, Ala154, Asp157 and Phe156, are also involved in the interaction between saquinavir and the ADRP domain. Saquinavir binds to the key catalytic residues that also participate in ADPr binding, indicating that saquinavir can inhibit the activity of the ADRP macrodomain and can potentially inhibit the Nsp3 protein of COVID-19. Saquinavir also interacts with several residues that are involved in ADPr binding in the crystal structure, showing that the drug is binding in the ADPr binding cavity and can act as a competitive inhibitor (Figure 2).

#### *ADRP-trifluoperidol*

Trifluoperidol was the second best hit in the virtual screen. The ADRP-trifluoperidol complex, which has a binding affinity of  $-10.2$  kcal/mol, is stabilized by three hydrogen bonds and several hydrophobic interactions. Gly48, Val49 and Phe156 form hydrogen bonds with trifluoperidol and a  $\pi$ - $\pi$  interaction was seen with Ile131. The complex was also stabilized by interactions with Asp22, Ile23, Ala38, Asn40, Gly46, Gly47, Gly51, Ala52, Pro125, Leu126, Ser128, Ala129, Gly130, Phe132, Ala154, Val155 and Asp157. Trifluoperidol binds to the key catalytic residues and shows higher binding affinity than ADPr, indicating its potential as an inhibitor of the ADRP macrodomain that can render the Nsp3 protein inactive. Several residues that interact with trifluoperidol are also involved in ADPr

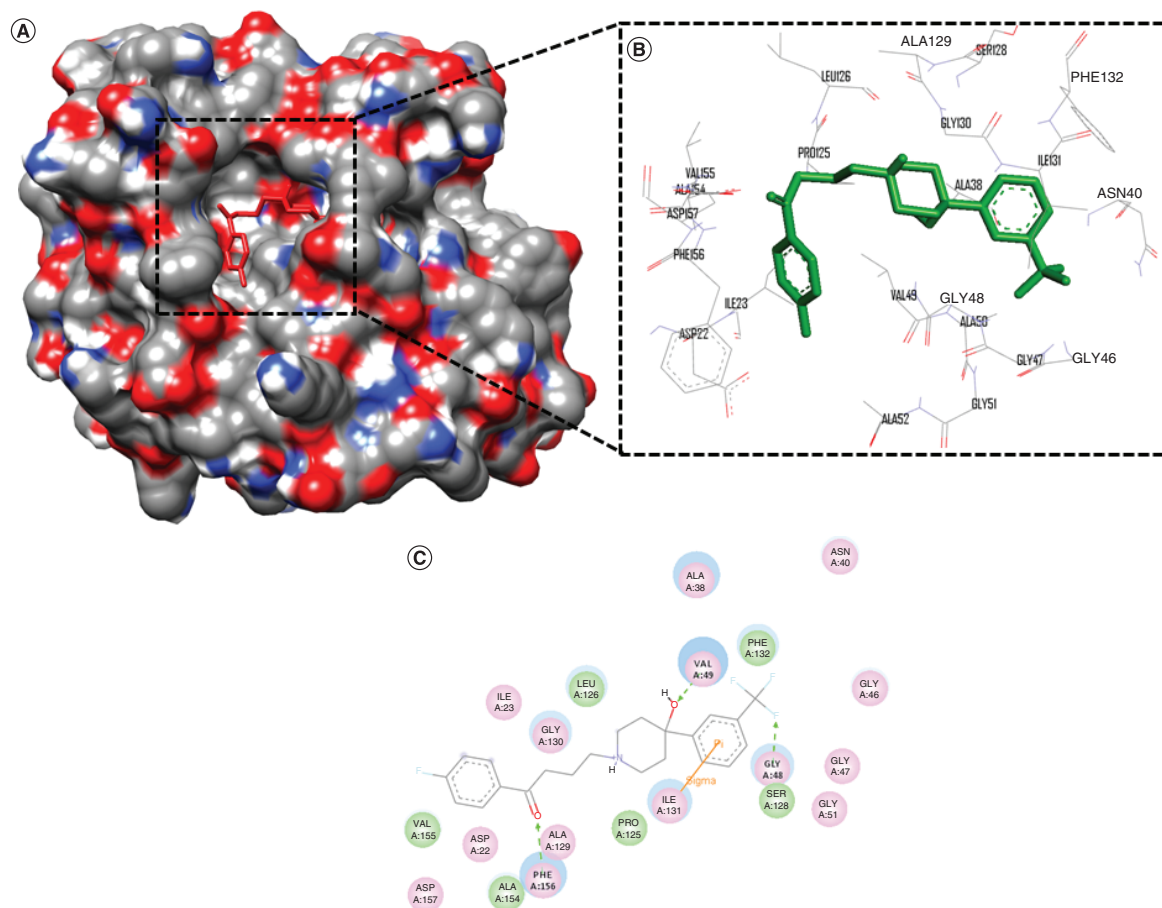


**Figure 3. Binding pattern of trifluoperidol with ADP-ribose phosphatase. (A)** Surface view of ADP-ribose phosphatase (ADRP)–trifluoperidol complex. **(B)** Residue interaction diagram of trifluoperidol with ADRP. **(C)** 2D-interaction diagram of ADRP–trifluoperidol interaction.

binding in the crystal structure, showing that the drug is binding in the ADPr binding cavity and can act as a competitive inhibitor (Figure 3).

#### *ADRP–deferasirox*

The ADRP–deferasirox complex, which has a binding affinity of  $-10.0$  kcal/mol and is among the top hits, is stabilized by various interactions, including one hydrogen bond with Gly130 and  $\pi$ - $\pi$  interaction with Ile131. Other residues, including Ala38, Gly48, Val49, Pro125, Leu126, Ser128, Ala129, Phe132, Gly133, Val155, Phe156, Asp157 and Leu160, stabilize the complex through various interactions. Deferasirox also binds to the key catalytic residues, indicating that it can also act as a good inhibitor of the ADRP macrodomain of Nsp3. Details are shown in Supplementary Figure 1.

#### *ADRP–droperidol*

Droperidol has a binding affinity of  $-10.0$  kcal/mol, calculated using Autodock Vina, and binds to various key catalytic residues, indicating that it also binds in the substrate binding cavity. Droperidol forms only one hydrogen bond, with Gly130, and numerous interactions with Ile23, Ala38, Gly48, Val49, Pro125, Leu126, Ser128, Ala129, Ile131, Phe132, Ala154, Val155, Phe156, Asp157 and Leu160 play a role in stabilizing this complex. Again, several residues involved in binding droperidol are also involved in ADPr binding in the crystal structure, indicating that the drug is binding in the ADPr binding cavity and can act as a competitive inhibitor. Details are shown in Supplementary Figure 2.

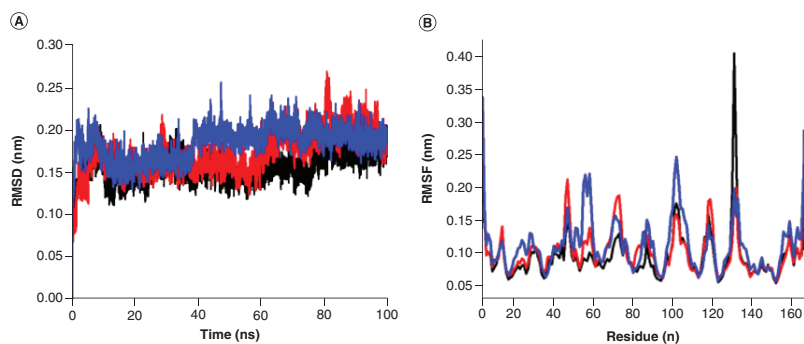


**Figure 4. Stability and flexibility analysis.** (A) Root mean square deviation of  $C\alpha$  backbone of ADP-ribose phosphatase (ADRP) and ligand complexes for 100 ns. (B) Root mean square fluctuation of  $C\alpha$  atoms of ADRP and ligand complexes. The black, red and blue represent ADRP-adenosine-5-diphosphoribose, ADRP-trifluperidol ADRP-saquinavir, respectively. RMSD: Root mean square deviation; RMSF: Root mean square fluctuation.

From these analyses, only two drugs (saquinavir and trifluperidol) were selected for further analysis because they showed good binding affinity for ADRP and bind in the deep groove containing the key catalytic residues. The ADRP-saquinavir and ADRP-trifluperidol complexes were compared with the ADRP-ADPr complex in the 100 ns MDS to analyze the stability of the protein–ligand complexes.

### Conformational analysis

The natural substrate (ADPr) and the two drugs with the highest binding affinity (saquinavir and trifluperidol) were used for MDS studies to investigate the binding mechanism, conformational dynamics and stability of the ADRP–ligand complexes. Three systems (ADRP–ADPr, ADRP–saquinavir and ADRP–trifluperidol) were prepared and used for the 100 ns MDS studies. Each system produced stable trajectories, which were then used for analysis. All the analyses were performed after the system attained equilibrium. Root mean square deviation (RMSD), root mean square fluctuation (RMSF), radius of gyration ( $R_g$ ), number of hydrogen bonds, SASA, PCA and binding free energy were calculated and analyzed.

#### *Stability analysis*

Deviation of the protein backbone from its initial state was calculated to determine structural stability. The calculated RMSD values were plotted for the whole duration of the 100 ns simulation of each system. The RMSD describes the conformational changes of a given protein over time. The complexes showed few differences at each time step, but the overall RMSD of each complex at any point of time was  $<0.26$  nm. The average RMSD values for the ADRP domain complexed with ADPr, trifluperidol and saquinavir were 0.147 nm, 0.164 nm and 0.175 nm, respectively. The RMSD values for each complex are thus comparable. The ADRP–ADPr complex showed the lowest average RMSD value of all the complexes, showing that the ADRP–substrate complex is slightly less stable than the ADRP–drug complexes. The overall patterns of the RMSD value (Figure 4A) are similar for the predicted drugs and the cocrystallized control ligand. The RMSD for each ligand was also calculated to predict ligand fluctuation in the binding pocket during the simulation. The average RMSD value of ADPr, trifluperidol and saquinavir were 0.31 nm, 0.23 nm and 0.30 nm, respectively. Slight conformational deviations in the ligand RMSD values of ADPr and saquinavir were observed, although each ligand formed a stable complex with ADRP during the simulation. Trifluperidol had a lower RMSD than saquinavir or ADPr, and saquinavir also showed a slightly lower RMSD than the control ligand. The overall RMSD results of the ADRP–ligand complexes and the unbound ligands showed that all trajectories reached equilibrium from the initial point of simulation and produced a stable trajectory throughout the analysis. In both analyses, trifluperidol had a lower RMSD value than saquinavir and was thus the more stable protein–ligand complex.

#### *Flexibility analysis*

RMSF values were calculated to investigate changes in flexibility of the protein after ligand binding. RMSF values should be high for well-organized structures, such as  $\alpha$ -helices and  $\beta$ -sheets and low for loosely organized structures, such as turns, coils and loops. The average RMSF values for ADRP complexes with ADPr, trifluperidol

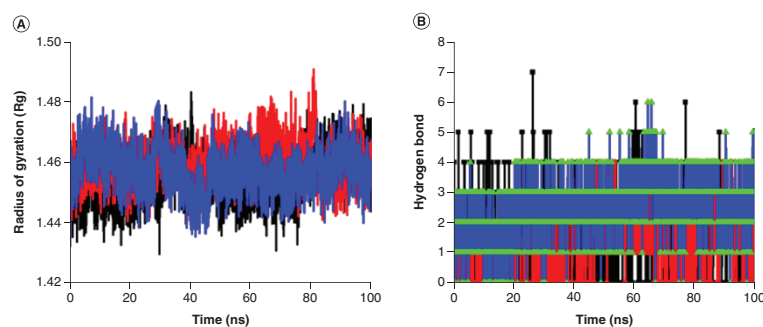


**Figure 5. Compactness and interaction analysis. (A)** Plot of radius of gyration versus time for ADP-ribose phosphatase (ADRP) with ligands. **(B)** Number of hydrogen bonds between protein and ligands. The black, red and blue represent ADRP-adenosine-5-diphosphoribose, ADRP-trifluperidol and ADRP-saquinavir respectively.

and saquinavir were 0.082 nm, 0.088 nm and 0.1 nm, respectively. These values, which are different for each protein–ligand complex, clearly indicate that ligand binding induces conformational changes in the ADRP domain (Figure 4B). The ADRP–ADPr complex showed the highest RMSF peak for residues 130 to 132, whereas the highest RMSF values for the ADRP–saquinavir complex were between residues 54–59 and 100–103, with a high deviation in the peak in the C-terminal region. The ADRP-trifluperidol complex showed high RMSF values for residues 45–47, 70–73 and 117–119. As seen in the docking section, some of these residues belong to the catalytic core of the ADRP domain. It is widely acknowledged that the native function of ADRP, or any other enzyme, requires a specific conformation and, as we can see from the RMSF results, drug binding alters the conformation and induces hindrances in the native dynamics of the protein. This means that ADRP cannot perform its native phosphatase activity, which may affect survival of the virus in the host because of inactivation of the Nsp3 enzyme. The RMSF results suggest that these drugs may inhibit ADRP activity and that the ADRP–trifluperidol complex is more stable than the ADRP–saquinavir complex.

#### Compactness analysis

Rg is the best parameter to describe the compactness of a protein after ligand binding. Rg values were predicted to investigate changes in compactness after ligand binding. It is assumed that smaller Rg values represent tightly packed protein structures, and vice versa. The average Rg values for ADRP complexes with ADPr, trifluperidol and saquinavir were 1.454 nm, 1.459 nm and 1.456 nm, respectively (Figure 5A). The pattern of Rg values was very similar for all the ADRP–ligand complexes, with only minor differences. This indicates that all the ADRP–ligand complexes are stable and compact throughout the simulation and that ligand binding does not induce major changes in the compactness of the ADRP domain. The average Rg values were ordered as follows: ADRP–ADPr complex < ADRP–saquinavir < ADRP–trifluperidol, indicating that all the complexes are stable and that saquinavir and trifluperidol may be used as lead compounds in the design of ADRP domain inhibitors.

#### Interaction analysis

Hydrogen bonds are very important interactions in protein–ligand complexes. Since they provide an indication of the stability of the protein–ligand complex, the number of hydrogen bonds in each complex was also calculated (Figure 5B). As shown in Figure 5B the ADRP–ADPr complex has the highest number of hydrogen bonds, and the ADRP–saquinavir complex has more hydrogen bonds than the ADRP–trifluperidol complex while average number of hydrogen bonds for ADRP–ADPr, ADRP–trifluperidol and ADRP–saquinavir was 2, 2 and 3, respectively. All the complexes thus had a good number of hydrogen bonds and were stable within the ADRP domain binding cavity throughout the simulation.

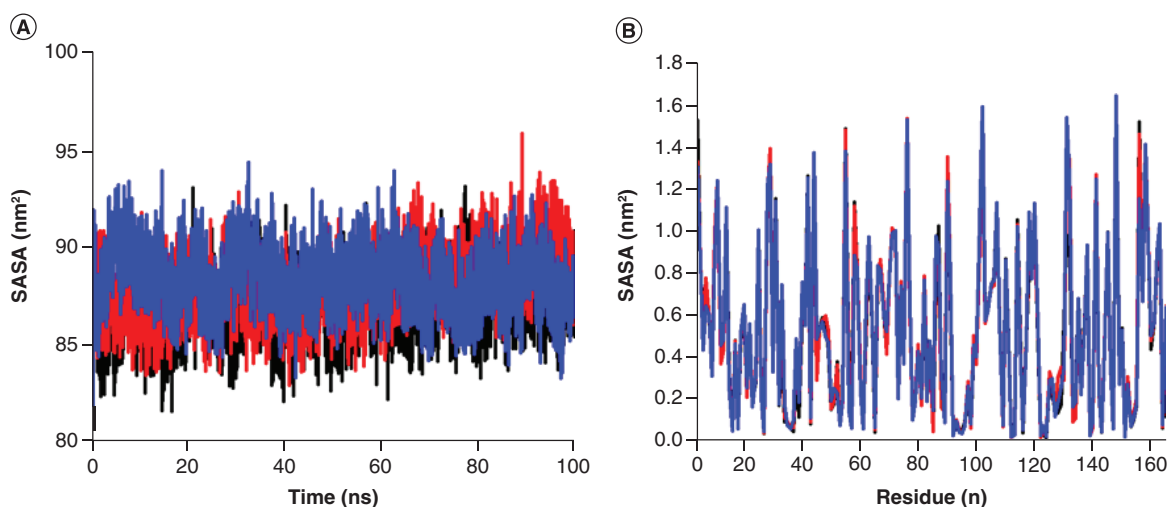


**Figure 6.** Solvent accessible surface area. (A) Solvent accessible surface area (SASA) value versus time for all the complex for 100 ns. (B) The residue versus SASA value for ADRP-ribose phosphatase (ADRP)-ligand complex. The black, red and blue represents ADRP-adenosine-5-diphosphoribose, ADRP-trifluoperidol and ADRP-saquinavir, respectively.

#### *Solvent accessible surface area analysis*

Values for SASA, which represent the area that is accessible to the solvent, were also calculated. SASA values were predicted to investigate ligand-induced changes in the ADRP domain (Figure 6A). The average values of SASA for both drugs were different from that of the control ligand ADPr, but the differences were not statistically significant. The average values of SASA for ADRP-ADPr, ADRP-trifluoperidol and ADRP-saquinavir were 86.94, 88.04, and 88.39 nm<sup>2</sup>, respectively. The SASA of the ADRP-trifluoperidol complex was thus smaller than that of the ADRP-saquinavir complex. Therefore both of the ADRP-drug complexes appear stable, and ADRP-trifluoperidol appears more stable than ADRP-saquinavir.

The residue SASA value, which indicates the SASA value on the basis of residues instead of time, was also calculated (Figure 6B). The average values for ADRP-ADPr, ADRP-trifluoperidol and ADRP-saquinavir were 0.52, 0.53, and 0.53 nm, respectively. The ADRP-saquinavir complex showed much greater fluctuation in several residues, compared with the other complexes. The ADRP-ADPr complex had a smaller residue SASA value, representing a more stable complex. The ADRP-trifluoperidol complex was also more stable than the ADRP-saquinavir complex.

#### *Principal component analysis*

PCA or essential dynamics analysis was performed to track changes in the correlated motions after ligand binding. Eigenvectors versus eigenvalues were calculated for the whole trajectory. The plots are shown in Figure 7A. Only the first 50 eigenvectors were included in the analysis for the best graphical representation, since the first eigenvectors represent the overall dynamics of the protein. The covariance matrix of atomic fluctuations was diagonalized to predict the eigenvalues. The plot shows the eigenvalue corresponding to each eigenvector for the ADRP-ADPr, ADRP-trifluoperidol and ADRP-saquinavir complexes. ADRP-ADPr showed the highest value for the first eigenvectors and ADRP-saquinavir showed the smallest value for first eigenvectors. The first eigenvector value of the ADRP-trifluoperidol complex lies between the values of the other two complexes. For further analysis, the first 10 eigenvectors were selected and the percentage motions for all three systems were calculated. The ADRP-ADPr, ADRP-trifluoperidol and ADRP-saquinavir complexes accounted for 70.29, 72.60, and 66.31%, respectively, of motions in the whole trajectory for the first 10 eigenvectors.

The first eigenvectors are very important for characterizing the overall essential dynamics of the protein-ligand complex. Therefore, the first eigenvectors were selected and plotted against each other (Figure 7B). The ADRP-trifluoperidol complex is stable because it did not show the abrupt pattern and did not cause very high fluctuations in the phase space. PCA thus suggests that both drugs form complexes with ADRP and that the ADRP-saquinavir complex is more stable.

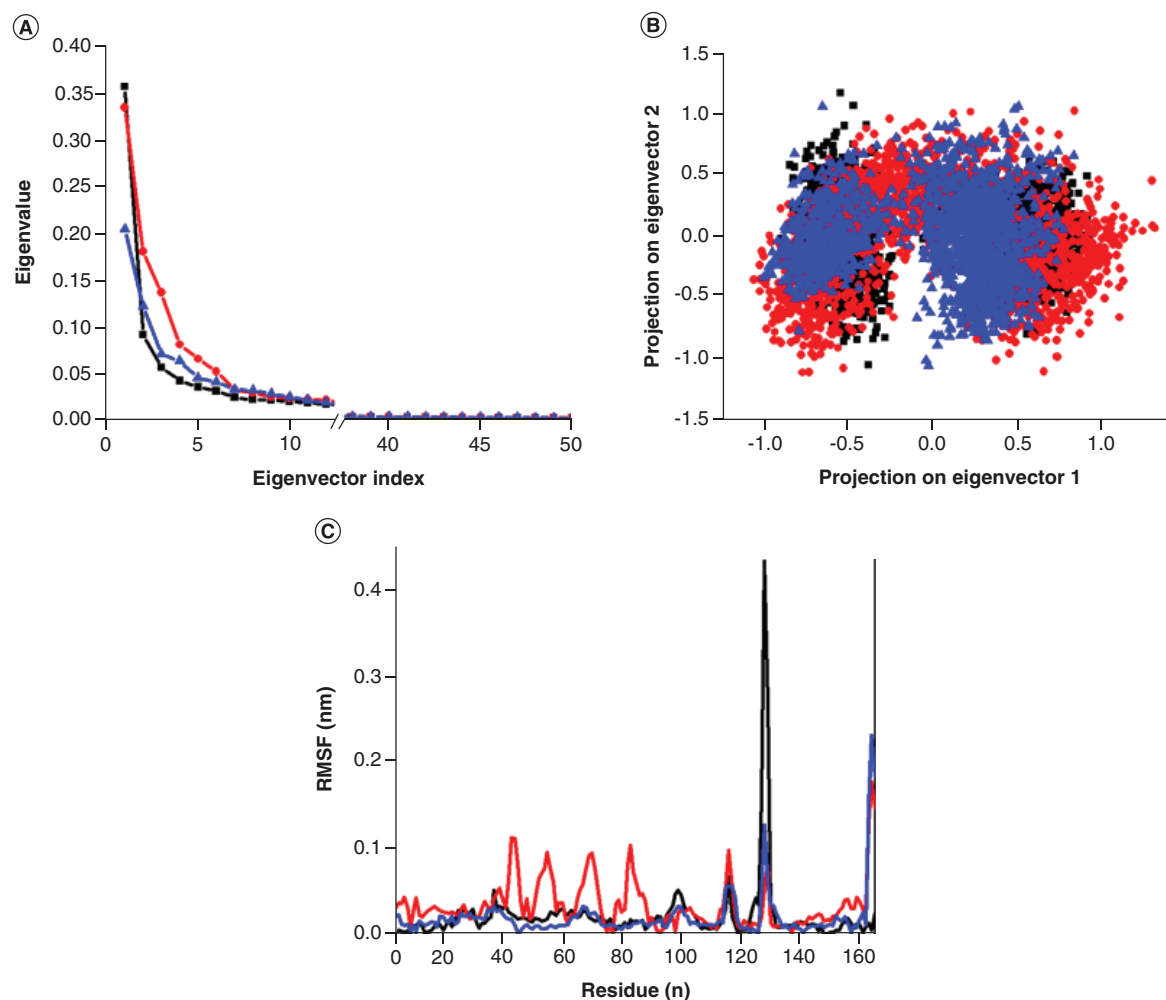


**Figure 7. Principal component analysis.** (A) First 50 eigenvectors were plotted versus eigenvalue for ADP-ribose phosphatase (ADRP)-ligand complexes. (B) Projection of the motion of the protein in phase space along PC1 versus PC2 for ADRP-ligand complexes. (C) The first eigenvector versus residue to see residue wise fluctuation. The black, red and blue represent ADRP-adenosine-5-diphosphoribose, ADRP-trifluperidol and ADRP-saquinavir, respectively.

Motions on the basis of residues were also calculated. The eigRMSF values were calculated only for first eigenvector on the basis of residues and are shown in Figure 7C. The average eig RMSF values for the ADRP-ADPr, ADRP-trifluperidol and ADRP-saquinavir complexes were 0.022, 0.034, and 0.021 nm, respectively. Compared with the other complexes, the ADRP-ADPr complex showed a very high eigRMSF value between residues 128–133. Trifluperidol also induced motions in residues 40–48, 50–60, 62–77 and 78–92. These residues are within the catalytic region of the protein and the result indicates that binding of trifluperidol alters the original conformation of the active site and induces conformational changes in the active site residues. Therefore, trifluperidol appears to be a good inhibitor of ADRP. The eig RMSF showed a similar pattern of residue fluctuation to the RMSF analysis.

#### *The Gibbs free energy landscape analysis*

The Gibbs free energy landscape, which inspects the spatial positions of atoms in a system, was calculated from PC1 and PC2 and plotted using Origin Software (Figure 8). A deeper blue color in the free energy landscape indicates lower energy. The graph shows two energy minima for the ADRP-ADP and ADRP-saquinavir complexes and multiple minima for the ADRP-trifluperidol complex. The ADRP-ADP and ADRP-saquinavir complexes reached two metastable conformations during the simulation and the ADRP-trifluperidol complex crossed multiple energy barriers to gain a metastable conformation. These results suggest that the ADRP-ADP, ADRP-saquinavir and ADRP-trifluperidol complexes are all stable.

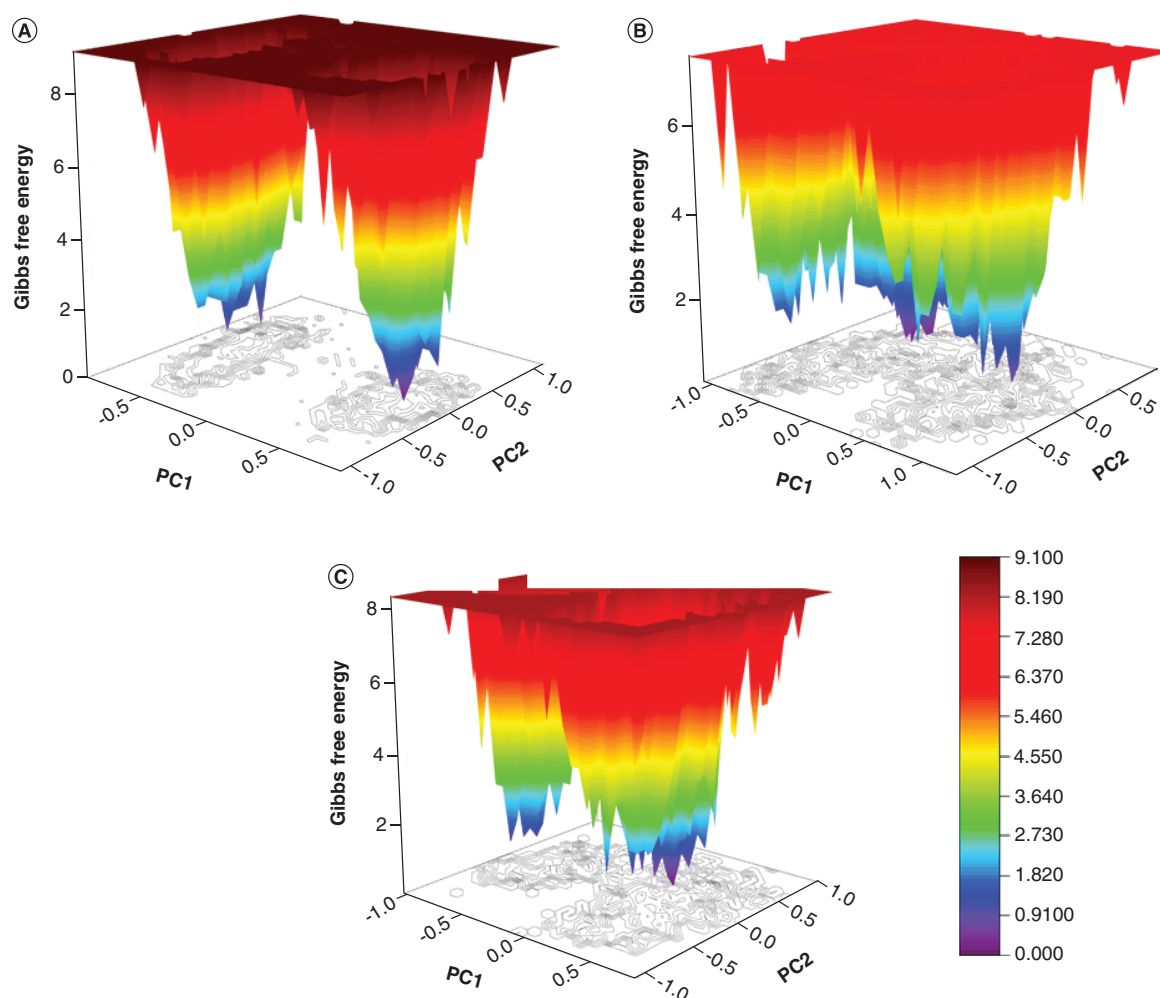


**Figure 8.** Gibbs free energy landscape. (A) ADP-ribose phosphatase (ADRP)–ADP complex. (B) ADPR–trifluoperidol. (C) ADPR–saquinavir.

**Table 3.** The Van der Waal, electrostatic, polar solvation, solvent accessible surface area and binding energy in  $\text{kJ mol}^{-1}$  for each complex.

Drug name	Van der Waal energy	Electrostatic energy	Polar solvation energy	SASA energy	Binding energy
ADP	$-104 \pm 83$	$-16 \pm 20$	$75 \pm 78$	$-9 \pm 8$	$-56 \pm 40$
Trifluoperidol	$-179 \pm 11$	$-15 \pm 9$	$100 \pm 9$	$-19 \pm 1$	$-114 \pm 13$
Saquinavir	$-75 \pm 109$	$-15 \pm 22$	$51 \pm 94$	$-8 \pm 11$	$-47 \pm 77$

SASA: Solvent-accessible surface area.

### Binding free energy analysis

The binding free energy was calculated for the last 5 ns trajectory snapshot. This method uses the polar and apolar solvation parameters to extract the binding affinity and gives the energy in several terms, including Vander Waals energy, electrostatic energy, polar solvation energy, SASA energy and average binding affinity. Detailed binding energies are shown in Table 3. The average binding affinities of the ADRP–ADP, ADRP–trifluoperidol and ADRP–saquinavir complexes were  $-56$ ,  $-114$ , and  $-47 \text{ kJ.mol}^{-1}$ , respectively. The ADRP–trifluoperidol complex thus has the highest binding affinity of all the complexes. The binding free energy results indicate that ADRP–trifluoperidol is the most stable complex and that trifluoperidol may act as a lead compound for the design of inhibitors of the ADRP domain.

## Discussion

COVID-19 is a newly emerged human-infectious coronavirus, a pandemic and a global health emergency. As COVID-19 cases are rising, there is an urgent need to design small compounds or inhibitors to cure COVID-19. The ARDP/Nsp3 is reported to be one of the key targets against COVID-19. There are several studies that have identified inhibitors against the ARDP/Nsp3. Debnath *et al.* conducted a virtual screening study against the ARDP where they took 113,687 compounds and screened them using the Glide XP docking tools [34]. From the selected compounds, the top six may act against the ARDP. Also, Lehrer *et al.* have suggested that haloperidol inhibitors can act as good inhibitors against COVID-19 [35]. The authors also suggest that trifluperidol can act as a novel inhibitor against the ARDP, which researchers should further characterize and validate. The current results agreed with the results of Lehrer *et al.*, as trifluperidol was also identified as an inhibitor from the pool of FDA-approved compounds in the current study. The PLpro domain is also a key target for which researchers have screened compounds by using structure-based virtual screening [36]. Further, Armstrong *et al.* have also identified inhibitors against the Nsp3 but they bind with the PLpro domain instead of ARDP domain [37]. They screened 1971 compounds against the Nsp3 domain and found that five compounds showed good  $IC_{50}$  against the PLpro while they did not show antiviral activity in the cellular SARS-CoV-2 infection assays. The researchers then blocked the PLpro activity by engineered competitive nanobodies.

These studies suggest that Nsp3 is a key target against the ARDP domain and blocking the activity of Nsp3 could lead to a good therapeutic approach. In the present study, we screened the available FDA-approved drugs against Nsp3 and selected the compounds that formed strong interactions with residues present in the binding groove of Nsp3. MD simulation studies and free energy calculations provided insights to the binding mechanism of the drugs to Nsp3 and showed trifluperidol as the best binder among all the identified hits. Trifluperidol is a butyrophenone-family derivative and was approved in the US for the treatment of psychosis in 1959. It acts by the inhibition of the dopamine receptors. Trifluperidol has other peripheral and central nervous system effects, producing both alpha adrenergic stimulation and blocking histamine and serotonin-mediated effects. But currently, due to the availability of a large variety of antipsychotic drugs, this drug has been terminated. Shim *et al.* showed that it can also inhibit the NMDA receptor and can cause side effects [38]. In this study, however, we selected all FDA-approved compounds including the butyrophenone derivatives and sorted on the basis of their binding affinity. We found that trifluperidol showed good binding affinity and can act as a better inhibitor despite its few side effects. This drug could be given to COVID-19 patients on the basis of their personal choice, upon further validation.

## Conclusion

The COVID-19 pandemic is spreading rapidly day by day across the globe. SARS-CoV-2 has multiple Nsps, of which Nsp3 is a multidomain complex that regulates RNA transcription. The macrodomain ADRP plays a key role in this process by removing ADP-ribose from ADP-ribosylated proteins and RNA. The ADRP domain can thus be regarded as a viable drug target. We screened 2892 FDA-approved compounds against the ADRP domain using the SBVS approach. The top twenty energy compounds were selected for further analysis. From these compounds, trifluperidol and saquinavir were chosen for further validation since they showed good binding affinity and interacted with the key catalytic residues of the macrodomain. The complexes of these two compounds with ADRP were compared with the ADP-ADRP complex in 100 ns MDS studies with various parameters, including RMSD, RMSF, Rg, SASA, number of hydrogen bonds and PCA. The results suggest that the ADRP-trifluperidol complex is more stable than the ADRP-saquinavir and ADP-ADRP complexes. We suggest that trifluperidol could be repurposed as an inhibitor of the catalytic activity of the ADRP domain of the Nsp3 protein to control the spread of COVID-19. We acknowledge that this is a computational study which is based on theoretical algorithms driven from practical knowledge and hope that experimental validation like binding assays and trials of this drug will be carried out by other scientists.

### Summary Points

- The COVID-19 pandemic is spreading rapidly across the globe. SARS-CoV-2 has multiple Nsps, of which Nsp3 is a multidomain complex that regulates RNA transcription.
- The macrodomain ADP-ribose phosphatase (ADRP) plays a key role in this process by removing ADP-ribose from ADP-ribosylated proteins; RNA belongs to the Nsp3 complex. The ADRP domain can thus be regarded as a viable drug target.
- We screened 2892 FDA-approved compounds against the ADRP domain using the SBVS approach.
- The top twenty energy compounds were selected for further analysis. From these compounds, trifluperidol and saquinavir were chosen for further validation since they showed good binding affinity and interacted with the key catalytic residues of the macrodomain.
- The complexes of these two compounds with ADRP were compared with the ADP-ADRP complex in 100 ns MDS studies with various parameters, including RMSD, RMSF, Rg, SASA, number of hydrogen bonds and PCA.
- The results suggest that the ADRP-trifluperidol complex is more stable than the ADRP-saquinavir and ADP-ADRP complexes.
- We suggest that trifluperidol could be repurposed as an inhibitor of the catalytic activity of the ADRP domain of the Nsp3 protein to control the spread of COVID-19.
- This was a computational study; experimental validation of this drug must be carried out by other scientists.

### Author contributions

A Panday performed all the experiments and drafted the manuscript.

### Supplementary data

To view the supplementary data that accompany this paper please visit the journal website at: [www.futuremedicine.com/doi/suppl/10.2217/fvl-2020-0233](http://www.futuremedicine.com/doi/suppl/10.2217/fvl-2020-0233)

### Financial and competing interests disclosure

The authors have no relevant affiliations or financial involvement with any organization or entity with a financial interest in or financial conflict with the subject matter or materials discussed in the manuscript. This includes employment, consultancies, honoraria, stock ownership or options, expert testimony, grants or patents received or pending, or royalties.

No writing assistance was utilized in the production of this manuscript.

### References

1. Zheng J. SARS-CoV-2: an emerging coronavirus that causes a global threat. *Int. J. Biol. Sci.* 16(10), 1678–1685 (2020).
2. Huang C, Wang Y, Li X *et al.* Clinical features of patients infected with 2019 novel coronavirus in Wuhan, China. *The Lancet* 395(10223), 497–506 (2020).
3. Wu F, Zhao S, Yu B *et al.* A new coronavirus associated with human respiratory disease in China. *Nature* 579(7798), 265–269 (2020).
4. Cui J, Li F, Shi Z-L. Origin and evolution of pathogenic coronaviruses. *Nat. Rev. Microbiol.* 17(3), 181–192 (2019).
5. Baez-Santos YM, St John SE, Mesecar AD. The SARS-coronavirus papain-like protease: structure, function and inhibition by designed antiviral compounds. *Antiviral Res.* 115, 21–38 (2015).
6. Lee HJ, Shieh CK, Gorbalenya AE *et al.* The complete sequence (22 kilobases) of murine coronavirus gene 1 encoding the putative proteases and RNA polymerase. *Virology* 180(2), 567–582 (1991).
7. Saikatendu KS, Joseph JS, Subramanian V *et al.* Structural basis of severe acute respiratory syndrome coronavirus ADP-ribose-1'-phosphate dephosphorylation by a conserved domain of nsP3. *Structure* 13(11), 1665–1675 (2005).
8. Grunewald ME, Chen Y, Kuny C *et al.* The coronavirus macrodomain is required to prevent PARP-mediated inhibition of virus replication and enhancement of IFN expression. *PLoS Pathog.* 15(5), e1007756 (2019).
9. Kuri T, Eriksson KK, Putics A *et al.* The ADP-ribose-1'-monophosphatase domains of SARS-coronavirus and human coronavirus 229E mediate resistance to antiviral interferon responses. *J. Gen. Virol.* 92, 1899–1905 (2011).
10. Michalska K, Kim Y, Jedrzejczak R *et al.* Crystal structures of SARS-CoV-2 ADP-ribose phosphatase (ADRP): from the apo form to ligand complexes. *bioRxiv* doi: <https://doi.org/10.1101/2020.05.14.096081> (2020) (Epub ahead of print).
11. Bahadur Gurung A, Ajmal Ali M, Lee J, Abul Farah M, Mashay Al-Anazi K. Structure-based virtual screening of phytochemicals and repurposing of FDA approved antiviral drugs unravels lead molecules as potential inhibitors of coronavirus 3C-like protease enzyme. *J. King Saud Univ. Sci.* 32(6), 2845–2853 (2020).

12. Padhi AK, Shukla R, Tripathi T. Rational design of the remdesivir binding site in the RNA-dependent RNA polymerase of SARS-CoV-2: implications for potential resistance. *bioRxiv* DOI:10.1101/2020.06.27.174896 (2020) (Epub ahead of print).
13. Rajendran V, Kandasamy S, Gupta A, Selvaraj J, Shivanandappa KC. In silico identification of potential antivirals and molecular dynamics against SARS-CoV2 main protease and RBD of spike protein. *ChemRxiv* DOI: 10.26434/chemrxiv.13181117.v1 (2020) (Epub ahead of print).
14. Pettersen EF, Goddard TD, Huang CC *et al.* UCSF Chimera – a visualization system for exploratory research and analysis. *J. Comput. Chem.* 25(13), 1605–1612 (2004).
15. Wishart DS, Feunang YD, Guo AC *et al.* DrugBank 5.0: a major update to the DrugBank database for 2018. *Nucleic Acids Res.* 46(D1), D1074–D1082 (2018).
16. Sterling T, Irwin JJ. ZINC 15 – ligand discovery for everyone. *J. Chem. Inf. Model* 55(11), 2324–2337 (2015).
17. O’Boyle NM, Banck M, James CA, Morley C, Vandermeersch T, Hutchison GR. Open Babel: an open chemical toolbox. *J. Cheminform.* 3, 33 (2011).
18. Shukla R, Munjal NS, Singh TR. Identification of novel small molecules against GSK3 $\beta$  for Alzheimer’s disease using chemoinformatics approach. *J. Mol. Graph. Model.* 91, 91–104 (2019).
19. Pathak RK, Gupta A, Shukla R, Baunthiyal M. Identification of new drug-like compounds from millets as Xanthine oxidoreductase inhibitors for treatment of Hyperuricemia: a molecular docking and simulation study. *Comput. Biol. Chem.* 76, 32–41 (2018).
20. Morris GM, Huey R, Lindstrom W *et al.* AutoDock4 and AutoDockTools4: automated docking with selective receptor flexibility. *J. Comput. Chem.* 30(16), 2785–2791 (2009).
21. Trott O, Olson AJ. AutoDock Vina: improving the speed and accuracy of docking with a new scoring function, efficient optimization, and multithreading. *J. Comput. Chem.* 31(2), 455–461 (2009).
22. Shukla R, Shukla H, Kalita P, Tripathi T. Structural insights into natural compounds as inhibitors of Fasciola gigantica thioredoxin glutathione reductase. *J. Cell. Biochem.* 119(4), 3067–3080 (2018).
23. Shukla H, Shukla R, Sonkar A, Tripathi T. Alterations in conformational topology and interaction dynamics caused by L418A mutation leads to activity loss of Mycobacterium tuberculosis isocitrate lyase. *Biochem. Biophys. Res. Commun.* 490(2), 276–282 (2017).
24. Rajendran V, Shukla R, Shukla H, Tripathi T. Structure-function studies of the asparaginyl-tRNA synthetase from Fasciola gigantica: understanding the role of catalytic and non-catalytic domains. *Biochem. J.* 475(21), 3377–3391 (2018).
25. Shukla R, Singh TR. High-throughput screening of natural compounds and inhibition of a major therapeutic target HsGSK-3 $\beta$  for Alzheimer’s disease using computational approaches. *J. Gen. Eng. Biotech.* 19(1), 61 (2021).
26. Abraham MJ, Murtola T, Schulz R *et al.* GROMACS: high performance molecular simulations through multi-level parallelism from laptops to supercomputers. *SoftwareX* 1–2, 19–25 (2015).
27. Schüttelkopf AW, van Aalten DMF. PRODRG: a tool for high-throughput crystallography of protein-ligand complexes. *Acta Crystallogr. D Biol. Crystallogr.* 60(Pt 8), 1355–1363 (2004).
28. Oostenbrink C, Villa A, Mark AE, van Gunsteren WF. A biomolecular force field based on the free enthalpy of hydration and solvation: the GROMOS force-field parameter sets 53A5 and 53A6. *J. Comput. Chem.* 25(13), 1656–1676 (2004).
29. Chandra A, Chaudhary M, Qamar I, Singh N, Nain V. In silico identification and validation of natural antiviral compounds as potential inhibitors of SARS-CoV-2 methyltransferase. *J. Biomol. Struct. Dyn.* 1–11 (2021).
30. Chandra A, Gurjar V, Qamar I, Singh N. Identification of potential inhibitors of SARS-COV-2 endoribonuclease (EndoU) from FDA approved drugs: a drug repurposing approach to find therapeutics for COVID-19. *J. Biomol. Struct. Dyn.* 1–11 (2020).
31. Pettersen EF, Goddard TD, Huang CC *et al.* UCSF Chimera – a visualization system for exploratory research and analysis. *J. Comput. Chem.* 25(13), 1605–1612 (2004).
32. Humphrey W, Dalke A, Schulten K. VMD: visual molecular dynamics. *J. Mol. Graph.* 14(1), 33–38 27–28 (1996).
33. Kumari R, Kumar R, Lynn A. g.mmpbsa – a GROMACS tool for high-throughput MM-PBSA calculations. *J. Chem. Inf. Model* 54(7), 1951–1962 (2014).
34. Debnath P, Debnath B, Bhaumik S, Debnath S. In silico identification of potential inhibitors of ADP-ribose phosphatase of SARS-CoV-2 nsP3 by combining e-pharmacophore- and receptor-based virtual screening of database. *ChemistrySelect* 5(30), 9388–9398 (2020).
35. Lehrer S, Rheinstein PH. SARS-CoV-2 orf1b gene sequence in the NTNG1 gene on human chromosome 1. *In Vivo* 34(Suppl. 3), 1629–1632 (2020).
36. Mitra D, Verma D, Mahakur B *et al.* Molecular docking and simulation studies of natural compounds of Vitex negundo L. against papain-like protease (PLpro) of SARS CoV-2 (coronavirus) to conquer the pandemic situation in the world. *J. Biomol. Struct. Dyn.* 18–1 (2020).
37. Armstrong LA, Lange SM, de Cesare V *et al.* Characterization of protease activity of Nsp3 from SARS-CoV-2 and its *in vitro* inhibition by nanobodies. *bioRxiv* doi: <https://doi.org/10.1101/2020.12.09.417741> (2020) (Epub ahead of print).
38. Shim SS, Grant ER, Singh S, Gallagher MJ, Lynch DR. Actions of butyrophenones and other antipsychotic agents at NMDA receptors: relationship with clinical effects and structural considerations. *Neurochem. Int.* 34(2), 167–175 (1999).